RESEARCH ARTICLE SUMMARY

NEURODEGENERATION

Heterochromatin anomalies and double-stranded RNA accumulation underlie *C9orf72* poly(PR) toxicity

Yong-Jie Zhang, Lin Guo, Patrick K. Gonzales, Tania F. Gendron, Yanwei Wu, Karen Jansen-West, Aliesha D. O'Raw, Sarah R. Pickles, Mercedes Prudencio, Yari Carlomagno, Mariam A. Gachechiladze, Connor Ludwig, Ruilin Tian, Jeannie Chew, Michael DeTure, Wen-Lang Lin, Jimei Tong, Lillian M. Daughrity, Mei Yue, Yuping Song, Jonathan W. Andersen, Monica Castanedes-Casey, Aishe Kurti, Abhishek Datta, Giovanna Antognetti, Alexander McCampbell, Rosa Rademakers, Björn Oskarsson, Dennis W. Dickson, Martin Kampmann, Michael E. Ward, John D. Fryer, Christopher D. Link, James Shorter, Leonard Petrucelli*

INTRODUCTION: Frontotemporal dementia (FTD) and amyotrophic lateral sclerosis (ALS) are fatal neurodegenerative diseases that share clinical and neuropathological features. Furthermore, the most common genetic cause of both FTD and ALS is a GGGGCC (G_4C_2) repeat expansion in the *C9orf72* gene. This repeat expansion leads to several abnormalities, including *C9orf72* haploinsufficiency, the accumulation of repeat RNA, and the production of five aggregation-prone proteins composed of repeating dipeptides. However, the contribution of these abnormalities to disease pathogenesis remains unresolved.

RATIONALE: Among the five dipeptide repeat proteins nonconventionally translated from expanded G_4C_2 repeats, proline-arginine (PR) repeat proteins [poly(PR) proteins] have proven especially toxic in various model systems. Their involvement in *C9orf72*-associated FTD and ALS (c9FTD/ALS) has nevertheless been questioned because poly(PR) pathology is relatively infrequent in c9FTD/ALS patient brains. Postmortem tissues, however, represent end-stage disease and do not necessarily reflect early events in the disease process. Therefore, we generated mice that express poly(PR) in the brain to evaluate the temporal consequences of its expression in a mammalian in vivo model. More specifically, we engineered mice to express green fluorescent protein (GFP)–conjugated $(PR)_{50}$ (a 50-repeat PR protein) or GFP via intracerebroventricular administration of adeno-associated viral vectors and then performed behavioral, pathological, and transcriptomic characterizations of poly(PR) mice in comparison with control GFP mice.

RESULTS: We found that ~60% of poly(PR)-expressing mice died by 4 weeks of age and had significantly decreased brain and body weights at death compared with age-matched GFP control mice. Poly(PR) mice that escaped premature death developed motor and memory impairments, likely as a consequence of their progressive brain atrophy, neuron loss, loss of poly(PR)-positive cells, and gliosis. In investigating the mechanisms by which poly(PR) caused neurodegeneration and functional deficits, we found that poly(PR) localized to heterochromatin (highly condensed regions of transcriptionally silent chromatin) and caused abnormal histone H3 methylation, features that we also detected in brain tissues from patients with c9FTD/ALS. Additionally, we observed aberrations in nuclear lamins and heterochromatin protein 1α (HP1α), key proteins that maintain heterochromatin structure and regulate gene silencing. Nuclear lamina invaginations and decreased HP1α protein expression were seen in poly(PR)-positive cells in poly(PR) mice, and in vitro studies demonstrated that poly(PR) disrupted HP1α liquid phases. Because poly(PR)-induced histone H3 posttranslational modifications, lamin invaginations, and decreased HP1α levels could profoundly affect gene expression, we compared transcriptome profiles between control and poly(PR) mice. As well as analyzing differentially expressed genes, we examined repetitive element expression given that repetitive DNA sequences make up a large portion of heterochromatin and that repetitive elements are substantially up-regulated in the brains of c9FTD/ALS patients. Whereas the majority of differentially expressed genes in poly(PR) mice were down-regulated, repetitive elements were markedly up-regulated, and this up-regulation was accompanied by the accumulation of double-stranded RNA. Furthermore, we confirmed that HP1α depletion caused double-stranded RNA accumulation in human induced pluripotent stem cell–derived neurons and decreased their survival.

ON OUR WEBSITE

Read the full article at http://dx.doi.org/10.1126/science.aav2606

CONCLUSION: Our studies provide compelling evidence that, by disrupting HP1α liquid phases, interacting with heterochromatin, and eliciting aberrant histone posttranslational modifications, poly(PR) adversely influences heterochromatin structure. Consequently, repetitive element expression is induced and double-stranded RNA accumulates, contributing to the neurodegeneration seen in patients with c9FTD/ALS. Rescuing histone methylation, lamin, and HP1α abnormalities and/or inhibiting abnormal repetitive element expression may represent promising therapeutic strategies for treating c9FTD/ALS. ■

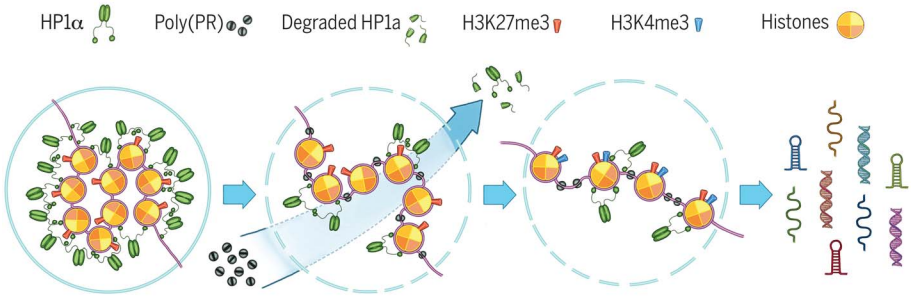

Poly(PR) interactions with heterochromatin cause repetitive element expression. Heterochromatin consists of tightly packed nucleosomes, DNA segments wound around histones. The *C9orf72*-associated dipeptide repeat protein poly(PR) disrupts HP1α liquid compartments on heterochromatin, thus evicting HP1α from heterochromatin and causing its degradation. Poly(PR) also binds heterochromatin and causes abnormal histone H3 methylation. These events alter heterochromatin structure and ultimately increase repetitive element expression and double-stranded RNA accumulation.

The list of author affiliations is available in the full article online.
*Corresponding author. Email: petrucelli.leonard@mayo.edu
Cite this article as Y.-J. Zhang *et al.*, *Science* **363**, eaav2606 (2019). DOI: 10.1126/science.aav2606

RESEARCH ARTICLE

NEURODEGENERATION

Heterochromatin anomalies and double-stranded RNA accumulation underlie *C9orf72* poly(PR) toxicity

Yong-Jie Zhang[1,2], Lin Guo[3], Patrick K. Gonzales[4], Tania F. Gendron[1,2], Yanwei Wu[1], Karen Jansen-West[1], Aliesha D. O'Raw[1], Sarah R. Pickles[1], Mercedes Prudencio[1,2], Yari Carlomagno[1], Mariam A. Gachechiladze[5], Connor Ludwig[6]*, Ruilin Tian[6], Jeannie Chew[1,2], Michael DeTure[1,2], Wen-Lang Lin[1], Jimei Tong[1], Lillian M. Daughrity[1], Mei Yue[1], Yuping Song[1], Jonathan W. Andersen[1], Monica Castanedes-Casey[1], Aishe Kurti[1], Abhishek Datta[7]†, Giovanna Antognetti[7], Alexander McCampbell[8], Rosa Rademakers[1,2], Björn Oskarsson[9], Dennis W. Dickson[1,2], Martin Kampmann[6], Michael E. Ward[5], John D. Fryer[1,2], Christopher D. Link[4], James Shorter[3], Leonard Petrucelli[1,2]‡

How hexanucleotide GGGGCC (G_4C_2) repeat expansions in *C9orf72* cause frontotemporal dementia (FTD) and amyotrophic lateral sclerosis (ALS) is not understood. We developed a mouse model engineered to express poly(PR), a proline-arginine (PR) dipeptide repeat protein synthesized from expanded G_4C_2 repeats. The expression of green fluorescent protein–conjugated $(PR)_{50}$ (a 50-repeat PR protein) throughout the mouse brain yielded progressive brain atrophy, neuron loss, loss of poly(PR)-positive cells, and gliosis, culminating in motor and memory impairments. We found that poly(PR) bound DNA, localized to heterochromatin, and caused heterochromatin protein 1α (HP1α) liquid-phase disruptions, decreases in HP1α expression, abnormal histone methylation, and nuclear lamina invaginations. These aberrations of histone methylation, lamins, and HP1α, which regulate heterochromatin structure and gene expression, were accompanied by repetitive element expression and double-stranded RNA accumulation. Thus, we uncovered mechanisms by which poly(PR) may contribute to the pathogenesis of *C9orf72*-associated FTD and ALS.

Frontotemporal dementia (FTD) and amyotrophic lateral sclerosis (ALS), two fatal neurodegenerative diseases, share neuropathological features, such as TAR DNA-binding protein 43 (TDP-43) pathology, and clinical symptoms. FTD patients typically present with progressive changes in behavior, executive function, and/or language caused by frontal and temporal lobe degeneration but can also develop ALS-like motor symptoms. Patients with ALS, which is caused by upper and lower motor neuron loss, develop muscle weakness, atrophy, and paralysis. In addition, ~50% of ALS patients experience cognitive and/or behavioral changes. The clinical and neuropathological overlap between FTD and ALS is accompanied by genetic overlap: A hexanucleotide GGGGCC (G_4C_2) repeat expansion in intron 1 of chromosome 9 open reading frame 72 (*C9orf72*) is the most common known genetic cause of FTD and ALS (*1*, *2*). The mechanisms by which *C9orf72* G_4C_2 repeat expansions cause *C9orf72*-associated FTD and ALS (c9FTD/ALS) are being extensively investigated. Mounting evidence implicates both loss-of-function and gain-of-function mechanisms in c9FTD/ALS pathogenesis. For instance, loss of C9ORF72 causes immune dysregulation (*3*, *4*) and impairs the autophagy-lysosome pathway (*5*–*9*), which may enhance abnormal protein deposition. The accumulation of expanded repeat-containing transcripts, conversely, is thought to cause toxic gains of function. These transcripts bind several RNA binding proteins and form RNA foci, thus impairing RNA metabolism (*10*–*14*), nucleocytoplasmic transport (*15*, *16*), and RNA transport granule function (*17*). Moreover, these transcripts produce glycine-alanine (GA), glycine-proline (GP), glycine-arginine (GR), proline-arginine (PR), and proline-alanine (PA) dipeptide repeat (DPR) proteins [poly(GA), poly(GP), poly(GR), poly(PR), and poly(PA)] through repeat-associated non-ATG translation (*18*–*22*). All five DPR proteins form neuronal inclusions in patients with c9FTD/ALS (*18*–*22*), but studies in cultured cells and neurons, as well as *Drosophila*, suggest that arginine-rich poly(PR) is the most toxic DPR protein (*23*–*32*). Several mechanisms have been ascribed to poly(PR)-induced toxicity, including nucleolar stress (*23*, *24*, *26*, *30*) and impaired nucleocytoplasmic transport (*27*, *28*), protein translation (*26*, *31*), and stress granule dynamics (*26*, *30*, *32*). Although poly(PR) is considered highly toxic, poly(PR) pathology is infrequent in c9FTD/ALS patient brains (*19*, *20*, *33*, *34*), raising questions about its contribution to c9FTD/ALS pathogenesis. However, because postmortem tissues represent end-stage disease and do not necessarily reflect early events in the disease process, we generated mice that express poly(PR) in the brain to evaluate the temporal consequences of poly(PR) expression in a mammalian in vivo model.

GFP-$(PR)_{50}$ mice developed neurodegeneration and behavioral deficits

We engineered mice to express green fluorescent protein (GFP)–conjugated $(PR)_{50}$ (a 50-repeat PR protein) or GFP in the brain via intracerebroventricular administration of adeno-associated virus serotype 1 (AAV1) at postnatal day 0. A codon-optimized vector was used to specifically express GFP-$(PR)_{50}$ in the absence of repeat RNA. Consistent with the reported toxicity of poly(PR) (*23*–*32*), ~60% of GFP-$(PR)_{50}$–expressing mice died by 4 weeks of age (fig. S1A) and had significantly decreased brain and body weights at death compared with age-matched GFP-expressing control mice (fig. S1, B to D). GFP-$(PR)_{50}$ mice that escaped premature death were sacrificed at 1 or 3 months of age for more in-depth analyses. These mice developed a progressive decrease in brain weight (fig. S2A), and hematoxylin- and eosin-stained brain sections revealed cortical thinning and reduced hippocampal volume in 3-month-old GFP-$(PR)_{50}$ mice compared with age-matched GFP mice (fig. S2B). With the exception of 3-month-old female mice, no difference in body weight was observed between age- and sex-matched GFP and GFP-$(PR)_{50}$ mice (fig. S2C).

Given that our gross morphological analysis revealed brain atrophy in GFP-$(PR)_{50}$ mice (fig. S2B), we examined the relationship between poly(PR) expression and neuron loss. Immunohistochemical staining showed a predominantly nuclear distribution of poly(PR) in the cortices and cerebellums of 1- and 3-month-old GFP-$(PR)_{50}$ mice (Fig. 1A and fig. S3A). Virtually all poly(PR)-positive cells were immunoreactive for the neuronal markers microtubule-associated protein 2 (MAP2) and NeuN, indicating that the poly(PR) expression was neuronal (fig. S3B). Notably, the number of poly(PR)-positive cells in the cortex and cerebellum significantly decreased from 1 to 3 months

[1]Department of Neuroscience, Mayo Clinic, Jacksonville, FL, USA. [2]Neuroscience Graduate Program, Mayo Clinic Graduate School of Biomedical Sciences, Jacksonville, FL, USA. [3]Department of Biochemistry and Biophysics, Perelman School of Medicine, University of Pennsylvania, Philadelphia, PA, USA. [4]Department of Integrative Physiology, Institute for Behavioral Genetics, University of Colorado, Boulder, CO, USA. [5]National Institute of Neurological Disorders and Stroke, National Institutes of Health, Bethesda, MD, USA. [6]Institute for Neurodegenerative Diseases, Department of Biochemistry and Biophysics, University of California, San Francisco, and Chan Zuckerberg Biohub, San Francisco, CA, USA. [7]Protein Chemistry, Biogen Idec, Cambridge, MA, USA. [8]Neurology Research, Biogen Idec, Cambridge, MA, USA. [9]Department of Neurology, Mayo Clinic, Jacksonville, FL, USA.
*Present address: Department of Bioengineering, Stanford University, Stanford, CA, USA. †Present address: Antibody Discovery, Scholar Rock, Cambridge, MA, USA.
‡Corresponding author. Email: petrucelli.leonard@mayo.edu

of age (Fig. 1, A and B, and fig. S3C). Consistent with these findings, immunoassay and immunoblot analyses showed a significant reduction in poly(PR) levels in 3-month-old GFP-$(PR)_{50}$ mice compared with 1-month-old GFP-$(PR)_{50}$ mice (Fig. 1C and fig. S3, D and E). The age-dependent loss of poly(PR)-expressing cells in the cortex and cerebellum was accompanied by an age-dependent loss of NeuN-positive cortical neurons (Fig. 1, D and E) and of cerebellar Purkinje cells (fig. S3, F and G), suggesting that poly(PR) expression caused cell-autonomous neuron death. Transgene RNA levels were significantly higher in GFP mice than in GFP-$(PR)_{50}$ mice, arguing against neuronal loss being caused by high transgene expression (fig. S3H).

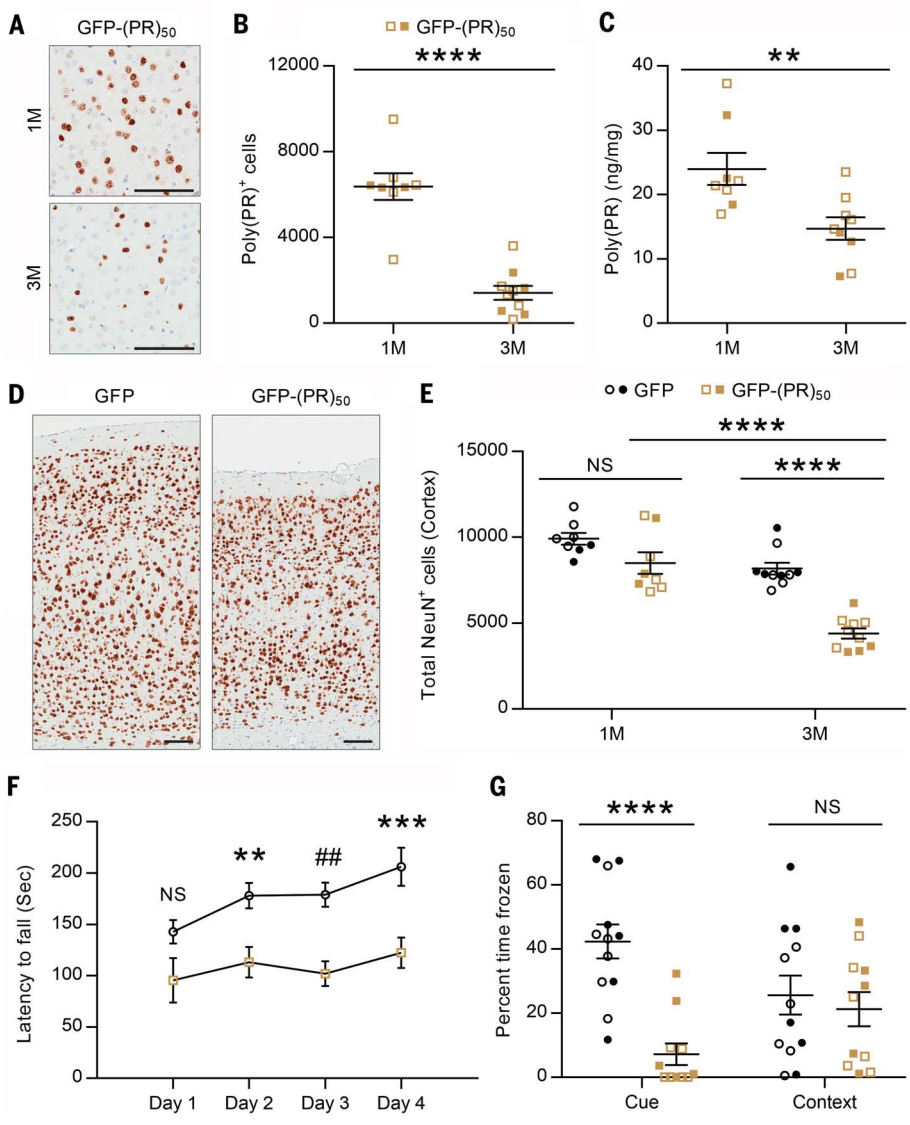

Fig. 1. GFP-$(PR)_{50}$ mice exhibited neurodegeneration and behavioral deficits. Immunohistochemical (**A**) and quantitative (**B**) analyses of anti-PR immunoreactivity in the cortices of GFP-$(PR)_{50}$ mice at 1 month (1M) (n = 8 mice) and 3 months (3M) (n = 10 mice) of age. Scale bars, 100 μm. (**C**) An immunoassay was used to compare poly(PR) levels in cortex and hippocampus lysates of GFP-$(PR)_{50}$ mice at 1 (n = 8 mice) and 3 (n = 9 mice) months of age. (**D**) Representative images of NeuN-labeled cells in the cortices of 3-month-old GFP or GFP-$(PR)_{50}$ mice. Scale bars, 100 μm. (**E**) Quantification of NeuN-labeled cells in the cortices of GFP mice at 1 (n = 8 mice) and 3 (n = 10 mice) months of age or GFP-$(PR)_{50}$ mice at 1 (n = 8 mice) and 3 (n = 10 mice) months of age. (**F**) Results from a 4-day rotarod test used to assess motor deficits of 3-month-old mice expressing GFP (n = 12 mice) or GFP-$(PR)_{50}$ (n = 11 mice) by evaluating their latency to fall from a rotating rod. (**G**) Results from the fear-conditioning test used to assess the associative learning and memory of 3-month-old mice expressing GFP (n = 12 mice) or GFP-$(PR)_{50}$ (n = 11 mice) by evaluating the percentage of time frozen in response to a conditioned (cued) or unconditioned (context) stimulus. Data are presented as the mean ± SEM. Male mice are represented by solid symbols, whereas female mice are represented by empty symbols. In (B) and (C), ****P < 0.0001, **P = 0.0072, two-tailed unpaired t test. In (E), ****P < 0.0001; NS (not significant), P = 0.1130; two-way ANOVA and Tukey's post hoc analysis. In (F), NS, P = 0.1269; **P = 0.0096; ##P = 0.0015; ***P = 0.0005; two-way ANOVA and Tukey's post hoc analysis. In (G), ****P < 0.0001; NS, P = 0.6007; two-tailed unpaired t test.

Inflammation is believed to be a key process in FTD and ALS and is often associated with neurodegeneration. Hence, we examined the brains of mice for reactive astrocytes and microglia. Transcript levels of *Gfap*, a marker of astrogliosis, were significantly increased in the brains of GFP-$(PR)_{50}$–expressing mice compared with those of GFP-expressing mice at 3 months of age, whereas no significant difference was observed at 1 month of age (fig. S4A). Transcript levels of *CD68*, a marker of activated microglia, were elevated at 1 and particularly 3 months of age in GFP-$(PR)_{50}$ mice (fig. S4A). Similar to RNA levels of *Gfap* and *CD68*, Gfap and CD68 protein expression in the cortices and cerebellums of 3-month-old GFP-$(PR)_{50}$ mice increased significantly, as confirmed by immunohistochemical analysis (fig. S4, B to E).

Examination of c9FTD/ALS behavioral features in 3-month-old GFP- or GFP-$(PR)_{50}$–expressing mice revealed both motor and cognitive deficits in the latter group (Fig. 1, F and G). On the rotarod test, GFP-$(PR)_{50}$ mice exhibited a decreased latency to fall compared with GFP mice (Fig. 1F), indicating impaired motor skills. GFP-$(PR)_{50}$ mice also displayed an associative memory deficit, as evidenced by a decrease in cued, but not contextual, freezing in a fear-conditioning task (Fig. 1G).

Poly(PR) proteins localized to heterochromatin and elicited aberrant posttranslational modifications of histone H3

Previous studies reported that poly(PR) causes cell death by accumulating in the nucleoli of cultured cells and neurons (*23*, *24*, *26*, *30*). Our GFP-$(PR)_{50}$–expressing mice provided an opportunity to investigate the mechanisms that underlie poly(PR)-induced neurotoxicity in vivo. We began by examining the cellular localization of poly(PR) in the brains of mice and found it to be present in a punctate pattern throughout the nucleus (Fig. 2A). Whereas some GFP-$(PR)_{50}$ colocalized with the nucleolar markers nucleophosmin (NPM1) and fibrillarin (Fig. 2A), the majority of GFP-$(PR)_{50}$ formed punctate structures that colocalized with the DNA-staining dye Hoechst 33258, suggestive of a heterochromatic distribution of poly(PR). Immunoelectron microscopy revealed that anti-poly(PR) antibodies decorated heterochromatin in the cortices of 3-month-old GFP-$(PR)_{50}$ mice (Fig. 2B) and purified mouse genomic DNA incubated with synthetic $(PR)_8$ peptides (Fig. 2C). Furthermore, electron microscopy showed that incubating genomic DNA with $(PR)_8$ or $(GR)_8$ peptides, but not $(GA)_8$, $(GP)_8$, or $(PA)_8$ peptides, changed DNA morphology, suggesting an electrostatic interaction between the negatively charged DNA and the positively charged $(PR)_8$ and $(GR)_8$ (Fig. 2C and fig. S5A). Electrophoretic mobility

shift assays also demonstrated that single- and double-stranded DNA bound to $(PR)_{20}$ and $(PR)_8$ peptides, thus forming higher-molecular-weight, less mobile complexes that were not observed when DNA was incubated with $(PA)_8$ peptides (Fig. 2D and fig. S5B).

To confirm that poly(PR) localized to heterochromatin in mice, cortical sections from 3-month-old GFP-$(PR)_{50}$ mice were co-stained for poly(PR) and the heterochromatin markers histone H3 lysine 9 trimethylation (H3K9me3) and histone H3 lysine 27 trimethylation (H3K27me3) or the euchromatin marker histone H3 lysine 4 trimethylation (H3K4me3) (Fig. 2E and fig. S5, C and D). These studies established that GFP-$(PR)_{50}$ essentially completely colocalized with heterochromatin markers (Fig. 2E and fig. S5C). Whereas the euchromatin marker H3K4me3 expectedly failed to colocalize with Hoechst 33258–stained heterochromatin in poly(PR)-negative cells, it did colocalize with heterochromatin and poly(PR) in GFP-$(PR)_{50}$–positive cells (Fig. 2E and fig. S5D). Moreover, levels of both the transcriptionally repressive H3K27me3 and the transcriptionally active H3K4me3 were increased in cells expressing poly(PR) compared with poly(PR)-negative cells in mice expressing GFP-$(PR)_{50}$ or GFP, and this was especially apparent for Hoechst 33258–stained pericentromeric heterochromatin (fig. S5, C to F). These data suggest that poly(PR) influences histone H3 posttranslational modifications. As in GFP-$(PR)_{50}$ mice, poly(PR) colocalized with H3K27me3 and H3K4me3 in the cortices of c9FTD/ALS patients (Fig. 2F, fig. S5G, and table S1). In fact, all nuclear poly(PR) inclusions detected in the cortices of patients with c9FTD/ALS colocalized with H3K27me3 and H3K4me3.

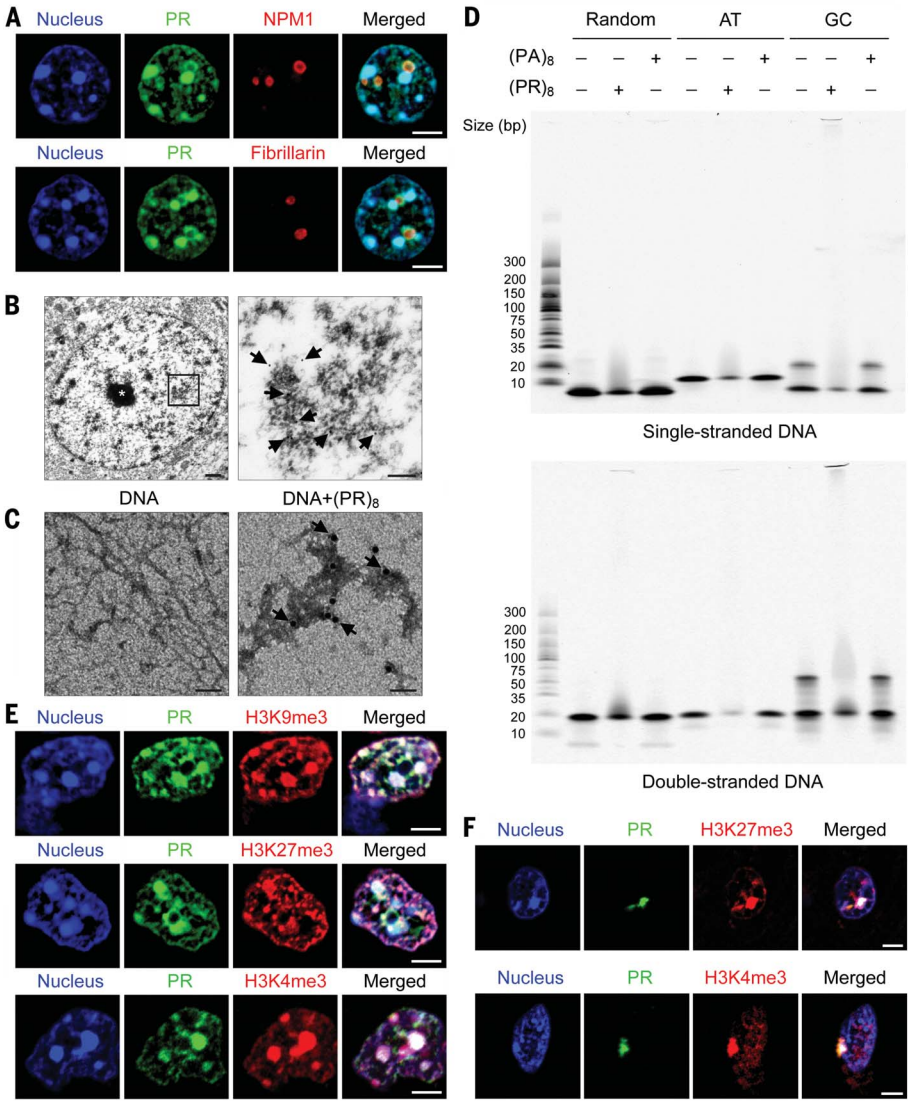

Fig. 2. Poly(PR) proteins localized to heterochromatin in GFP-$(PR)_{50}$ mice and c9FTD/ALS patients. (**A**) Double immunofluorescence staining for GFP-$(PR)_{50}$ and nucleolar markers (NPM1 and fibrillarin) in the cortices of 3-month-old GFP-$(PR)_{50}$ mice (n = 5). Scale bars, 5 μm. (**B**) Immunoelectron microscopy using an anti-PR antibody labeled with gold particles in the cortices of 3-month-old GFP-$(PR)_{50}$ mice. The selected region in the low-magnification image (left) is shown at high magnification (right). * indicates the nucleolus. Arrows indicate gold particles. Scale bars, 0.5 μm (left) and 0.2 μm (right). (**C**) Immunoelectron microscopy analysis of purified mouse genomic DNA incubated with $(PR)_8$ peptide by using an anti-PR antibody labeled with gold particles. Arrows indicate gold particles. Scale bars, 50 nm. (**D**) Electrophoretic mobility shift assays using single- and double-stranded DNA co-incubated (+) or not (−) with $(PR)_8$ or $(PA)_8$ peptides. AT, AT-rich oligonucleotides; GC, GC-rich oligonucleotides. (**E**) Double immunofluorescence staining for GFP-$(PR)_{50}$ and heterochromatin (H3K9me3 and H3K27me3) or euchromatin (H3K4me3) markers in the cortices of 3-month-old GFP-$(PR)_{50}$ mice (n = 7). Scale bars, 5 μm. (**F**) Double immunofluorescence staining for poly(PR) and H3K27me3 or H3K4me3 in the cortices of c9FTD/ALS patients. All nuclear poly(PR) inclusions colocalized with H3K27me3 (n = 7 cases) and with H3K4me3 (n = 4 cases). Representative images from case 4 are shown. See also fig. S5F and table S1. Scale bars, 5 μm.

Poly(PR) proteins caused nuclear lamina invaginations, reduced HP1α protein expression, and disrupted HP1α liquid phases

Next, we investigated the influence of poly(PR) on heterochromatin structure by examining the lamins and heterochromatin protein 1α (HP1α), key proteins in establishing and maintaining heterochromatin structure (*35*–*38*). Staining of mouse brain sections for lamins A/C and B showed a significantly higher frequency of nuclear lamina invaginations in cells expressing poly(PR) than in poly(PR)-negative cells in mice expressing GFP-$(PR)_{50}$ or GFP (Fig. 3A and fig. S6A). Moreover, we noted that cells expressing poly(PR) showed markedly decreased expression of HP1α protein (Fig. 3B and fig. S6B) but not HP1α mRNA (fig. S6C). Rather, a modest increase in HP1α mRNA was observed, which may reflect a compensatory mechanism. By contrast to HP1α, HP1β remained unchanged in poly(PR)-positive cells (fig. S6D). Despite the finding that $(GR)_8$, like $(PR)_8$, changed DNA morphology in vitro (fig. S5A), HP1α protein levels were not altered in GFP-$(GR)_{100}$ mice (fig. S6E), nor does poly(GR) influence lamin distribution in mice (*39*). Because poly(GR) does not localize to the nucleus, these data suggest that poly(PR)-induced alterations of lamins and HP1α are caused by the heterochromatic distribution of poly(PR) within the nucleus.

Poly(PR) may cause decreases in HP1α by impairing lamin function (*40*–*42*) and may also influence HP1α more directly, given that both poly(PR) and HP1α localize to heterochromatin. HP1α undergoes liquid-liquid phase separation (LLPS), with liquid HP1α compartments sequestering compacted chromatin and promoting heterochromatin-mediated gene silencing (*43*, *44*). Poly(PR) interferes with the LLPS of RNA binding proteins with prionlike domains and promotes aberrant phase transitions from liquid droplets to solid aggregates (*26*). Thus, we examined whether poly(PR) disrupted preformed HP1α liquid droplets in vitro to mimic in vivo conditions

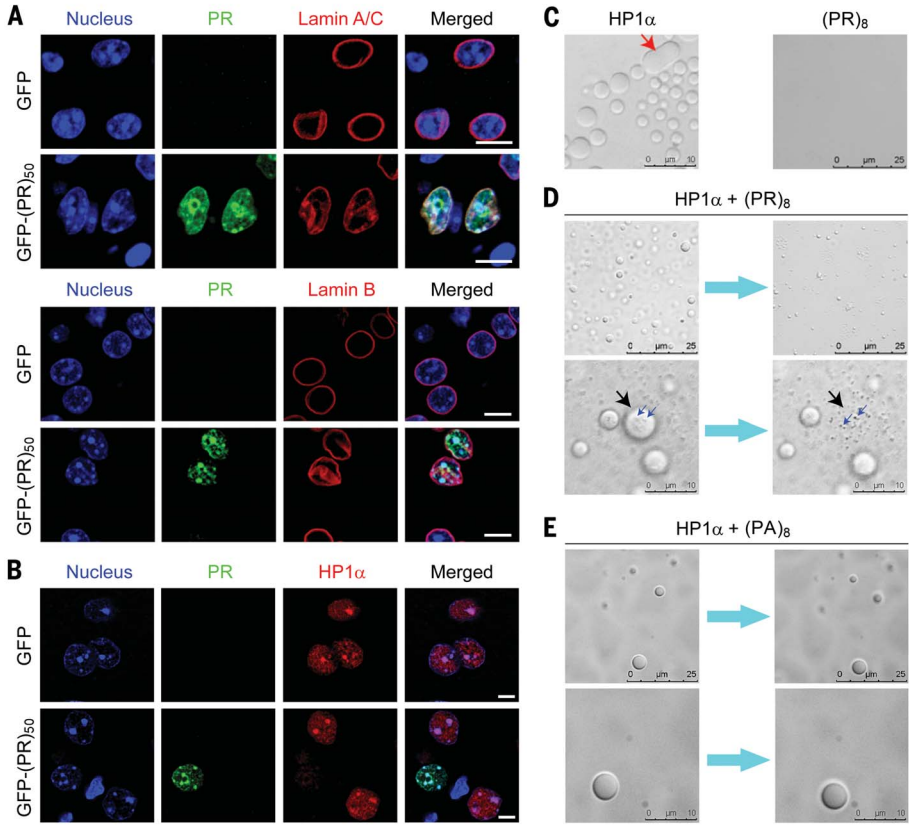

Fig. 3. Poly(PR) proteins caused lamin invaginations, reduced HP1α levels, and disrupted HP1α liquid droplets. (**A**) Double immunofluorescence staining for GFP-$(PR)_{50}$ and lamin A/C or lamin B in the cortices of 3-month-old GFP (n = 11) or GFP-$(PR)_{50}$ (n = 7) mice. Scale bars, 10 μm. (**B**) Double immunofluorescence staining for GFP-$(PR)_{50}$ and HP1α in the cortices of 3-month-old GFP-$(PR)_{50}$ mice (n = 7). Scale bars, 5 μm. (**C**) Differential interference contrast (DIC) microscopy images of HP1α droplets at a concentration of 90 μM HP1α before the addition of $(PR)_8$. The arrow indicates the fusing of two liquid droplets. By contrast, $(PR)_8$ peptides at a concentration of 245 μM did not form droplets under these conditions. (**D**) DIC microscopy images of HP1α droplets at 90 μM HP1α (top, low magnification; bottom, high magnification) after the addition of 245 μM $(PR)_8$. Black arrows indicate the bursting of a preformed HP1α droplet after the addition of $(PR)_8$. Small blue arrows indicate the solid components within HP1α droplets. (**E**) DIC microscopy images of HP1α droplets at 90 μM HP1α (top, low magnification; bottom, high magnification) after the addition of 245 μM $(PA)_8$ peptides. In (D) and (E), turquoise arrows between images indicate progression over time.

when poly(PR) encounters liquid HP1α compartments on heterochromatin. We first assembled HP1α droplets, spherical structures that readily underwent fusion consistent with liquidlike properties (Fig. 3C, arrow). To these HP1α liquid droplets, we added $(PR)_8$, which under these conditions did not phase separate in isolation (Fig. 3C). Initially, $(PR)_8$ rapidly induced the formation of solid components (Fig. 3D, blue arrows), which were not observed before the addition of $(PR)_8$ (Fig. 3C), inside the HP1α liquid droplets. HP1α droplets then violently burst to release these solid components (Fig. 3D, black arrows, and movie S1). After incubation with $(PR)_8$, few HP1α droplets remained (Fig. 3D). By contrast, $(PA)_8$ had no effect on preformed HP1α liquid droplets (Fig. 3E and movie S2). Thus, $(PR)_8$ but not $(PA)_8$ rapidly elicited an aberrant phase transition within HP1α droplets and caused their rupture. We suggest that this mechanism directly disrupts HP1α liquid compartments on heterochromatin, thereby evicting and depleting HP1α from heterochromatin, where it is replaced by poly(PR) in vivo.

Poly(PR) enhanced repetitive element expression and caused the accumulation of double-stranded RNA

Given that poly(PR) elicited aberrant post-translational modifications of histone H3 and caused lamin invagination and decreases in HP1α protein, which are expected to influence gene expression, we compared transcriptome profiles between 3-month-old mice expressing GFP or GFP-$(PR)_{50}$. Clustering of the 1000 most variable genes showed distinct expression profiles for GFP-$(PR)_{50}$ and GFP mice (Fig. 4A). Of the 2196 genes that were differentially expressed in GFP-$(PR)_{50}$ mice, the majority (1552) were down-regulated (Fig. 4B and dataset S1). Weighted gene coexpression network analysis of differentially expressed genes with a merging distance of 0.01 identified 13 modules, all of which were significantly associated with genotype after adjustment for multiple tests (Fig. 4C and dataset S1). Gene Ontology enrichment analysis across these modules identified the pink and blue modules as the most significantly enriched. Within the pink module, molecular function and biological process analyses, respectively, identified top terms specific to unfolded protein binding ($P = 2.13 \times 10^{-8}$; Bonferroni correction = 8.77×10^{-5}) and protein folding ($P = 3.05 \times 10^{-9}$; Bonferroni correction = 3.63×10^{-5}). Within the blue module, molecular function, cellular component, and biological process analyses, respectively, identified top terms specific to the structural constituent of the ribosome ($P = 9.26 \times 10^{-8}$; Bonferroni correction = 3.81×10^{-4}), ribosome biogenesis ($P = 1.86 \times 10^{-6}$; Bonferroni correction = 2.21×10^{-2}), and the ribosomal subunit ($P = 2.26 \times 10^{-6}$; Bonferroni correction = 3.75×10^{-3}). These pathways have been implicated in c9FTD/ALS (*26*, *31*, *39*, *45*, *46*).

In addition to identifying differentially expressed genes in GFP-$(PR)_{50}$ mice, we examined the expression of repetitive elements (REs) given our findings that poly(PR) localized to heterochromatin and that repetitive DNA sequences, which make up a large portion of heterochromatin (*47*), are significantly up-regulated in the brains of patients with c9ALS (*48*). By using a combination of RepEnrich2 and DESeq2, we identified a total of 1067 RepeatMasker-derived REs belonging to multiple repeat classes (dataset S2). Notably, the proportions of REs in distinct classes were comparable among GFP, GFP-$(PR)_{50}$, and GFP-$(GR)_{100}$ mice (table S2). In GFP-$(PR)_{50}$ mice compared with control GFP mice, 172 REs were differentially expressed [false discovery rate (FDR) < 0.10], with ~92% of these being up-regulated (Fig. 5A). This marked up-regulation of REs contrasted with the down-regulation of the majority of differentially expressed genes (Fig. 4B). Quantitative polymerase chain reaction (qPCR) analysis of select RE hits confirmed their up-regulation (Fig. 5B and fig. S7A). No specific classes of REs were enriched, indicating a global change in their expression. Of note, no RE was differentially expressed in mice expressing GFP-$(GR)_{100}$ (fig. S7B). Because RE transcripts were elevated in GFP-$(PR)_{50}$ mice and because these transcripts can form double-stranded RNA (dsRNA) (*49*–*51*), we evaluated whether dsRNA was produced in GFP-$(PR)_{50}$ mice. Immunofluorescence staining with an antibody against dsRNA revealed that dsRNA was specifically increased in cells expressing poly(PR) (Fig. 5C and fig. S7C). Accumulation of dsRNA was not observed in mice expressing GFP-$(GR)_{100}$ (fig. S7D).

A previous study found that the deletion of HPL-2, a *Caenorhabditis elegans* ortholog of HP1α, leads to the accumulation of dsRNA (*52*). To further determine whether the reduction of HP1α in GFP-$(PR)_{50}$ mice contributed to the observed accumulation of dsRNA, we repressed HP1α transcription in human cells by CRISPR interference

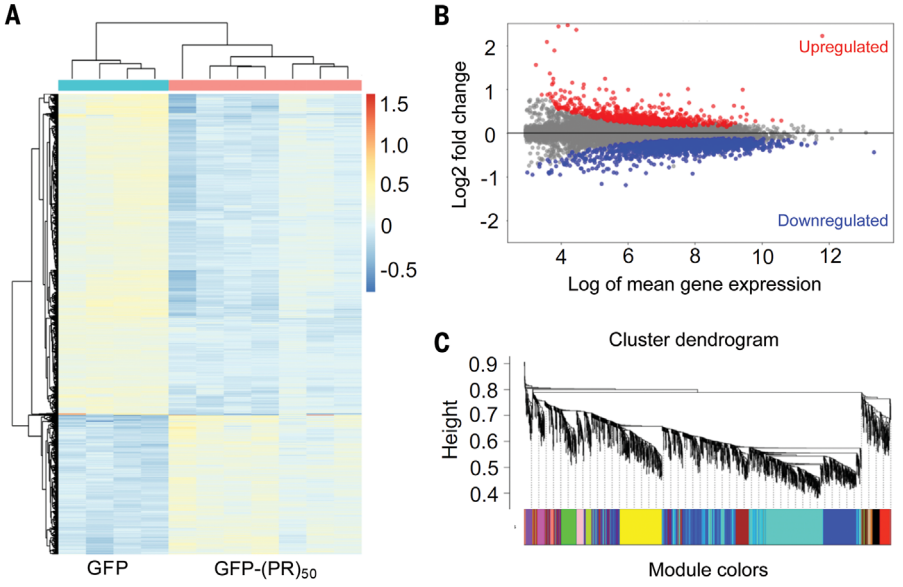

Fig. 4. Transcriptome alterations were identified in the brains of mice expressing GFP-$(PR)_{50}$. (**A**) Hierarchical clustering of the 1000 most variable genes between 3-month-old GFP mice (n = 4) and GFP-$(PR)_{50}$ mice (n = 7). (**B**) MA plots of up- and down-regulated genes (FDR < 0.01) in the cortices and hippocampi of 3-month-old mice expressing GFP-$(PR)_{50}$ (n = 7) compared with those of GFP controls (n = 4). The MA plot is based on the Bland-Altman plot, where M represents the $\log_2$ fold change (y axis) and A represents the log of mean gene expression (x axis). (**C**) Gene modules identified in brains of 3-month-old mice expressing GFP-$(PR)_{50}$ (n = 7 mice) through weighted gene coexpression correlation network analyses using differentially expressed genes.

(CRISPRi), which is highly specific compared with RNA interference–based approaches (*53*, *54*). To this end, we individually transduced human induced pluripotent stem cells (iPSCs) stably expressing nuclease-deactivated CRISPR-associated protein 9 fused to blue fluorescent protein and the KRAB repressor domain (dCas9-BFP-KRAB) (*55*) with five single guide RNAs (sgRNAs) predicted to mediate CRISPRi of the HP1α gene. Because sgRNA 1 had the greatest ability to decrease HP1α protein expression (fig. S7E), we differentiated dCas9-BFP-KRAB iPSC cells expressing HP1α sgRNA 1 into neurons. HP1α sgRNA 1 caused a ~40% reduction of HP1α RNA, as assessed by qPCR (fig. S7F). Notably, dsRNA accumulated only in iPSC-differentiated neurons depleted of HP1α (Fig. 5D). Moreover, cells positive for dsRNA showed immunoreactivity for active caspase-3 (Fig. 5E), suggesting that dsRNA is toxic to neurons.

Poly(PR) caused abnormalities in nucleocytoplasmic transport proteins

Earlier studies have demonstrated that poly(PR) aberrantly affects nuclear pores and impairs nucleocytoplasmic transport in cultured cells and yeast models (*27*, *28*). Because poly(PR) caused lamin invagination in poly(PR) mice (Fig. 3A and fig. S6A), which may affect nuclear membrane integrity, we investigated whether poly(PR) also perturbs the nucleocytoplasmic transport factor Ran guanosine triphosphatase–activating protein 1 (RanGAP1) and nuclear pore complex (NPC) proteins, the latter assessed by using an antibody that recognizes Phe-x-Phe-Gly (where x is usually a small residue such as Ser, Gly, or Ala) nucleoporin repeats. We observed abnormal nuclear membrane invaginations immunopositive for RanGAP1 or NPC proteins in poly(PR)-positive cells compared with poly(PR)-negative cells in mice expressing GFP-$(PR)_{50}$ or GFP (Fig. 6 and fig. S8A). RanGAP1 was abnormally distributed in virtually all poly(PR)-positive cells (Fig. 6A and fig. S8A), whereas NPC protein abnormalities in poly(PR)-positive cells were less frequent (Fig. 6B).

Given that defects in RanGAP1 may impair the nucleocytoplasmic transport of TDP-43 and promote its cytoplasmic accumulation, we evaluated whether poly(PR) caused TDP-43 pathology, a hallmark feature of c9FTD/ALS. However, similar to mice expressing poly(GA) or poly(GR) (*39*, *56*), poly(PR)-expressing mice did not develop TDP-43 inclusions, suggesting that the expression of individual DPR proteins is insufficient to cause TDP-43 pathology within the time frames examined (Fig. 6C and fig. S8B). Additional pathological mechanisms associated with poly(PR) include stress granule formation and nucleolar stress (*23*, *24*, *26*, *30*). Nevertheless, no evidence of stress granules was seen in the brains of GFP-$(PR)_{50}$ mice (fig. S8C). This may be due to the absence of cytoplasmic poly(PR) inclusions, which, similar to poly(GR) cytoplasmic inclusions, have been shown to initiate stress granule formation and sequester stress granule–associated proteins (*26*, *39*). Likewise, although nucleolar poly(PR) was occasionally observed in GFP-$(PR)_{50}$ mice, no sign of nucleolar stress (i.e., repressed ribosomal RNA expression) was detected (fig. S8, D and E), suggesting that nucleolar poly(PR) levels must reach a threshold to induce nucleolar stress.

Discussion

In this study, we found that poly(PR) expression in the brain caused premature death in ~60% of mice, with surviving GFP-$(PR)_{50}$ mice developing age-dependent brain atrophy and neuron loss, as well as impaired motor and memory functions. GFP-$(PR)_{50}$ mice that succumbed to an early death exhibited higher poly(PR) levels than surviving mice (37.89 ± 11.88 versus 23.99 ± 7.071 ng/mg; P = 0.0367, two-tailed unpaired t test), indicative that poly(PR) toxicity is dose dependent. The age-dependent neuron loss in surviving mice was accompanied by a similar age-dependent loss of poly(PR)-positive cells, suggesting that poly(PR)-positive neurons progressively degenerated. These data are consistent with the results of a study showing that poly(PR) expression causes cultured neurons to die in a time-dependent fashion (*24*) and may also explain, at least in part, why poly(PR) pathology is rare in postmortem brain tissues from c9FTD/ALS patients (*19*, *20*, *33*, *34*), which reflect the end stage of disease.

The neurodegeneration and behavioral deficits of GFP-$(PR)_{50}$ mice were associated with the localization of poly(PR) to heterochromatin, highly condensed regions of transcriptionally silent chromatin (*47*). A heterochromatic localization of poly(PR) was also observed in c9FTD/ALS patients. Both increased H3K27me3, which represses gene expression, and increased H3K4me3, which activates gene expression, were observed in the heterochromatin of poly(PR)-expressing cells. Although the mechanism(s) by which poly(PR) elicited aberrant posttranslational modifications of histone H3 remain to be determined, these data suggest that poly(PR) causes epigenetic changes, which may influence heterochromatin function in c9FTD/ALS. Our RNA-sequencing (RNA-seq) and qPCR analyses of GFP-$(PR)_{50}$ mouse brain tissues revealed that RE sequences, which are enriched in heterochromatin DNA, were significantly up-regulated. Poly(PR)-induced RE expression in cultured cells was also evident through the accumulation of dsRNA, which can be formed by REs (*49*–*51*). The expression of REs, which is observed in several neurodegenerative diseases, is associated with neurotoxicity (*49*, *57*, *58*). Increased RE expression (*48*) and dsRNA accumulation (*57*) occur in c9FTD/ALS patients, and we reported previously that increases in general transcription may contribute to this enhanced RE expression (*48*). It is thus noteworthy that despite the marked up-regulation of REs in GFP-$(PR)_{50}$ mice, the majority of differentially expressed genes were down-regulated. Therefore, data from our GFP-$(PR)_{50}$ mice suggest that poly(PR) plays a role in RE expression in c9FTD/ALS but does so through heterochromatin alterations rather than enhanced transcription.

To more thoroughly evaluate how poly(PR) causes abnormal RE expression, we investigated

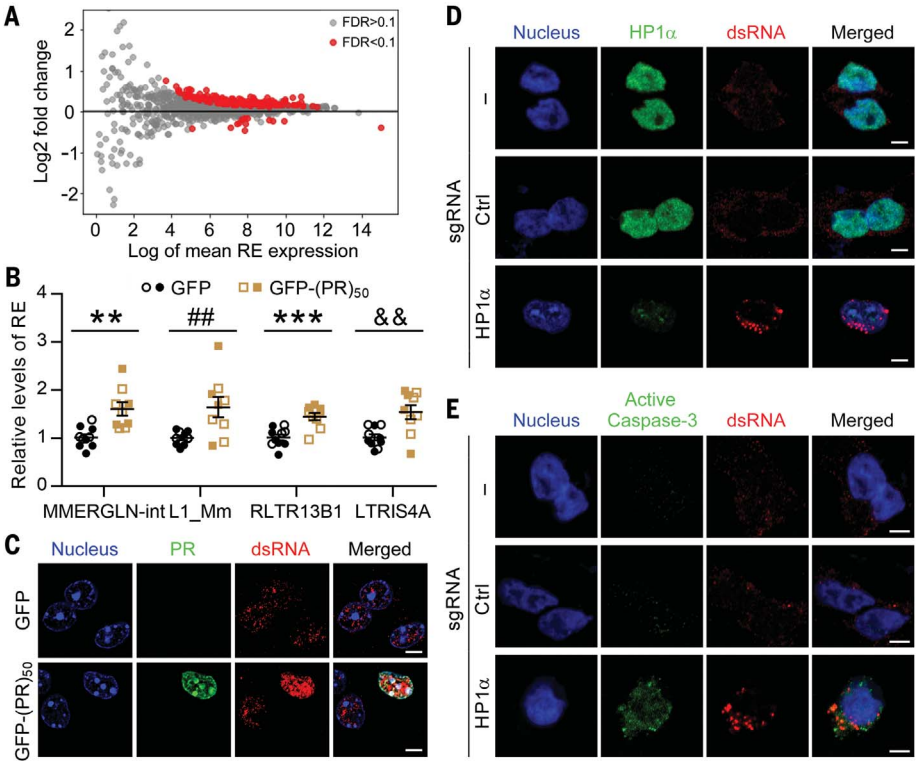

Fig. 5. Poly(PR) caused abnormal expression of REs and dsRNA accumulation. (**A**) MA plots of RNA-seq data show up- and down-regulated REs in the cortices and hippocampi of 3-month-old GFP-$(PR)_{50}$ mice (n = 7) compared with GFP mice (n = 4). Red dots represent the REs with a significant change (FDR < 0.10). (**B**) Validation of REs identified by RNA-seq in the cortices and hippocampi of 3-month-old GFP (n = 10) or GFP-$(PR)_{50}$ (n = 9) mice by qPCR. (**C**) Double immunofluorescence staining for GFP-$(PR)_{50}$ and dsRNA in the cortices of 3-month-old GFP mice (n = 3) or GFP-$(PR)_{50}$ mice (n = 7). Scale bars, 5 μm. (**D**) Double immunofluorescence staining for HP1α and dsRNA in human dCas9-iPSC–differentiated neurons stably expressing HP1α sgRNA 1. Scale bars, 5 μm. Ctrl, control. (**E**) Double immunofluorescence staining for active caspase-3 and dsRNA in human dCas9-iPSC–differentiated neurons stably expressing HP1α sgRNA 1. Scale bars, 5 μm. Data are presented as the mean ± SEM. Male mice are represented by solid symbols, whereas female mice are represented by empty symbols. In (B), $^{**}P$ = 0.0015; $^{\#\#}P$ = 0.0065; $^{***}P$ = 0.0004; and $^{\&\&}P$ = 0.0036; two-tailed unpaired t test.

lamins and HP1α, key proteins in establishing and maintaining heterochromatin structure and in regulating gene silencing (*35*–*38*). Lamin dysfunction and/or loss of HP1α causes heterochromatin relaxation and mitigates gene silencing, which result in the increased expression of DNA REs within heterochromatin regions (*35*–*38*). It is thus of interest that the localization of poly(PR) to heterochromatin coincided with lamin invaginations and decreased HP1α expression in the brains of GFP-$(PR)_{50}$ mice. Whereas poly(PR) may cause HP1α depletion indirectly by inducing lamin dysfunction (*40*–*42*), it may also directly disrupt HP1α liquid compartments on heterochromatin, thereby evicting HP1α and rendering it vulnerable to degradation. Our data raise the following possible scenario: poly(PR) ruptures HP1α liquid phases on heterochromatin, interacts directly with DNA, and accumulates on heterochromatin. In turn, the disruption of HP1α liquid phases leads to lamin invaginations and HP1α depletion, which cause increased RE expression and dsRNA accumulation. In support of this, we confirmed that the knockdown of HP1α in human iPSC-differentiated neurons resulted not only in the accumulation of dsRNA but also in caspase-3 activation, a marker of apoptosis.

Although further studies are needed to delineate the precise mechanism by which poly(PR) causes lamin invaginations, one potential cause or consequence is defects in nucleocytoplasmic transport proteins, which have previously been implicated in c9FTD/ALS (*15*, *28*, *56*). We observed that RanGAP1 was abnormally distributed in all poly(PR)-positive cells in GFP-$(PR)_{50}$ mice, and NPC protein abnormalities were also found, albeit less frequently. The exact contribution of these phenomena to the neurodegeneration and behavioral deficits of GFP-$(PR)_{50}$ mice remains to be resolved.

Overall, our studies provide compelling evidence that, by interacting with DNA, eliciting aberrant histone posttranslational modifications, and disrupting HP1α liquid phases, poly(PR) adversely influences heterochromatin structural organization. Consequently, RE expression is induced and dsRNA accumulates, contributing to the neurodegeneration seen in patients with c9FTD/ALS. Rescuing histone methylation, lamin, and HP1α abnormalities and/or inhibiting the abnormal expression of REs may represent promising therapeutic strategies for treating c9FTD/ALS.

Materials and methods summary

Detailed materials and methods can be found in the supplementary materials.

Generation of plasmids

To generate the AAV-GFP-$(PR)_{50}$ plasmid, a pEGFP-C1-$(PR)_{50}$ plasmid produced in our previous study (*59*) was subcloned into a modified AAV packaging vector containing the cytomegalovirus (CMV)–enhanced chicken β-actin promoter and the enhanced GFP (EGFP) coding sequence. To generate the HP1α-His plasmid, cDNA of an HP1α fragment was ligated to the NdeI and XhoI restriction sites of a pET-30a vector (69909-3, EMD Millipore). To generate Lenti-HP1α-sgRNA plasmids, we chose five sgRNA sequences against HP1α (CBX5) described in a previous study (*60*). The forward and reverse oligonucleotides were annealed and then ligated to the BstXI and BlpI restriction sites of a pU6-sgRNA EF1Alpha-puro-T2A-BFP vector (*53*). The sequence of GFP-$(PR)_{50}$ and primer sequences for cloning are listed in tables S3 and S4, respectively.

Virus production

To produce recombinant AAV1 (rAAV1) virus, AAV vectors expressing GFP or GFP-$(PR)_{50}$ were cotransfected with helper plasmids in human embryonic kidney (HEK) 293T cells. Cells were harvested 72 hours after transfection and lysed in the presence of 0.5% sodium deoxycholate (SDS) by freeze thawing, and the virus was isolated by using a discontinuous iodixanol gradient. The genomic titer of each virus was determined by qPCR. To produce lentivirus, HEK293T cells were cotransfected with plasmids of HP1α-sgRNA, psPAX2 (12260, Addgene), pMD2.G (12259, Addgene), and pAdVAntage (E1711, Promega) by using Lipofectamine 2000 (11668-019, Thermo Fisher Scientific). Media containing virus were harvested, filtered, and used to transduce dCas9-iPSCs.

Approvals

All procedures using mice were performed in accordance with the National Institutes of Health *Guide for the Care and Use of Laboratory Animals* (*61*) and approved by the Mayo Clinic Institutional Animal Care and Use Committee (protocol number A42014).

Neonatal viral injections

Intracerebroventricular injections of virus in postnatal-day-0 C57BL/6J pups were performed as previously described by using 2 μl (1×10^{10} genomes/μl) of AAV1-GFP or AAV1-GFP-$(PR)_{50}$ solution per cerebral ventricle (*39*, *56*).

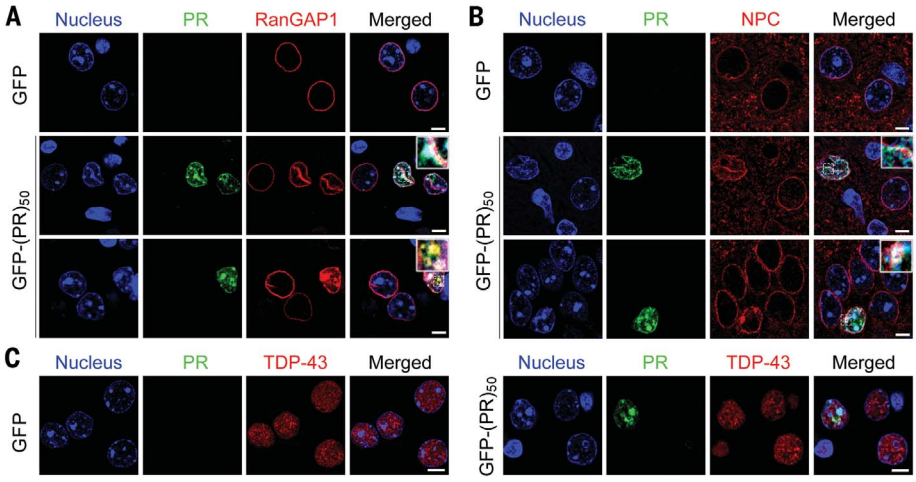

Fig. 6. Expression of GFP-$(PR)_{50}$ in mice caused abnormalities of RanGAP1 and NPC proteins but did not lead to TDP-43 pathology. (**A**) Double immunofluorescence staining for GFP-$(PR)_{50}$ and RanGAP1 in the cortices of 3-month-old GFP (n = 11) or GFP-$(PR)_{50}$ (n = 7) mice. Scale bars, 5 μm. (**B**) Double immunofluorescence staining for GFP-$(PR)_{50}$ and NPC proteins in the cortices of 3-month-old GFP or GFP-$(PR)_{50}$ mice (n = 4 mice per group). Scale bars, 5 μm. Insets in (A) and (B) show boxed areas at higher magnification. (**C**) Double immunofluorescence staining for GFP-$(PR)_{50}$ and TDP-43 in the cortices of 3-month-old GFP or GFP-$(PR)_{50}$ mice (n = 3 mice per group). Scale bars, 5 μm.

Behavioral tests

Three-month-old mice expressing GFP (n = 12 mice) or GFP-$(PR)_{50}$ (n = 11 mice) were subjected to behavioral analysis in two consecutive weeks by the Mayo Mouse Behavior Core. On two consecutive days of week 1, mice were subjected to tests of contextual and cued fear conditioning. On four consecutive days of week 2, the mice were subjected to the rotarod test. A detailed description of these tests is provided in the supplementary materials.

Tissue processing

For RNA, protein, and immunostaining analyses, mice were euthanized by CO_2 and brains were harvested and cut sagittally across the midline. Sagittal half brains were immersion fixed in 10% formalin, embedded in paraffin, sectioned (to 5 μm thick), and mounted on glass. The cortex and hippocampus of the other half brain were dissected and frozen on dry ice. Frozen mouse cortex and hippocampus tissues were homogenized in ice-cold tris-EDTA (TE), pH 8.0, with 2× protease and phosphatase inhibitors. Homogenates were used for RNA or protein extractions. For immunoelectron microscopy studies, mice were anesthetized with sodium ketamine and xylazine and then perfused with 0.9% saline followed by 4% paraformaldehyde. Brains were harvested, cut sagittally across the midline, and placed in 4% paraformaldehyde.

Preparation of brain protein lysates

To prepare protein lysates, 10% Triton X-100 and 10% SDS were added to brain homogenates at final concentrations of 1% and 2%, respectively. Homogenates were sonicated on ice and then centrifuged at 16,000 × g for 20 min. Supernatants were collected as lysates, and protein concentrations were determined by a bicinchoninic acid (BCA) assay (23225, Thermo Fisher Scientific). Protein lysates were used for Western blot and immunoassay analyses as described in the supplementary materials by using antibodies listed in table S5.

Human tissues

Postmortem frontal cortical tissues from FTD and ALS patients with *C9orf72* repeat expansions were obtained from the Mayo Clinic Florida Brain Bank. Information on human patients is provided in table S1. Written informed consent was obtained from all subjects or their legal next of kin if they were unable to give written consent, and biological samples were obtained with Mayo Clinic Institutional Review Board approval.

Immunohistochemistry and immunofluorescence staining

Paraffin sections of mouse and human brains were subjected to immunohistochemistry and immunofluorescence staining as previously described (*39*, *56*). Detailed methods for staining conditions, information on primary antibodies used, and quantification of neuropathology are provided in the supplementary materials and table S5.

Electrophoretic mobility shift assays

To analyze the binding of $(PR)_{20}$, $(PR)_8$, or $(PA)_8$ to single- or double-stranded DNA, Cy3-labeled random, CG-rich, or AT-rich oligonucleotides were incubated with the peptides before samples were resolved on 4 to 20% tris-borate EDTA (TBE) gels (Invitrogen) as described in the supplementary materials.

Postembedding immunoelectron microscopy

To examine the localization of poly(PR) proteins in mouse brain, immunoelectron microscopy was performed (*56*, *59*). Thin sections were pretreated with sodium citrate buffer, and then rabbit polyclonal poly(PR) antibody (1:50) was used as the primary antibody and goat anti-rabbit immunoglobulin G (IgG) conjugated with 18-nm colloidal gold particles (1:20, Jackson ImmunoResearch Laboratories) was used as the secondary antibody. Thin sections stained with uranyl acetate and lead citrate were examined with a Philips 208S electron microscope (FEI) fitted with a Gatan 831 Orius charge-coupled device (CCD) camera.

RNA extraction, reverse transcription, and qPCR

To extract total RNA in mouse brain, 1 volume of brain homogenate was mixed with 3 volumes of Trizol LS reagent (10296010, Thermo Fisher Scientific) and frozen on dry ice. One day later, total RNA was extracted by using the Direct-zol RNA MiniPrep kit (R2073, Zymo Research). To extract total RNA from iPSC-differentiated neurons, cell pellets were lysed in TRI reagent and then total RNA was extracted by using the Direct-zol RNA MiniPrep kit. cDNA was obtained by reverse transcription PCR by using 1000 ng of RNA with random primers and a high-capacity cDNA transcription kit (4368814, Applied Biosystems). To quantify RNA levels of the indicated transcripts in mouse brain or cultured cells, qPCR was conducted as described in the supplementary materials. Primer sequences are listed in table S6. Relative RNA expression levels of *Gfap*, *CD68*, and *HP1α* were normalized to *Gapdh* or *GAPDH* values (endogenous transcript controls).

RNA-seq, Gene Ontology, and repetitive element analyses

The library preparation and RNA-seq were performed by the Mayo Clinic Sequencing Core Facility (Rochester, MN) as previously described (*39*) and as detailed in the supplementary materials. After the preparation of the libraries, samples were subjected to quality control, cluster generation, and sequencing on the Illumina HiSeq 2000 platform. All reads had a read length of 100 bp and were paired-end. The number of reads per sample is listed in table S7. Weighted gene coexpression network analysis, the Gene Ontology overrepresentation test, differential expression analysis, and RE analysis were performed as described in the supplementary materials.

Purification of recombinant HP1α proteins

HP1α-His plasmid was used for transformation in Rosetta(DE3)pLysS competent cells (709563, EMD4Biosciences). To induce the expression of recombinant proteins, bacteria were cultured overnight at 16°C in the presence of 0.5 mM isopropyl β-D-1-thiogalactopyranoside. After centrifugation, the bacterial pellet was washed, lysed, sonicated, and centrifuged. The resulting supernatant was applied to a HisTrap HP histidine-tagged protein purification column (17524801,

GE Healthcare), and the recombinant proteins were eluted, desalted, and concentrated.

In vitro DPR protein and HP1α assays

HP1α liquid droplets (90 μM monomer) were formed in buffer containing 50 mM tris, pH 7.5. The preformed HP1α droplets were spotted onto a coverslip and imaged for 5 min, and then 245 μM $(PR)_8$ or $(PA)_8$ peptides were added to the sample and the sample was imaged for another 5 to 10 min.

i^{3}N iPSC culture and neuronal differentiation

We modified a well-characterized control iPSC line (WTC11) that harbors a dox-inducible NGN2 transgene at the AAVS1 locus (i^{3}N) (*62*, *63*). dCas9-BFP-KRAB was stably expressed in these i^{3}N iPSCs via TALEN-mediated integration of a CAG-dCas9-BFP-KRAB expression cassette into the CLYBL safe harbor locus (*55*). The dCas9-BFP-KRAB iPSCs were transduced with lentivirus expressing HP1α-sgRNA for 3 days and then selected by the addition of puromycin. To differentiate i^{3}N dCas9-BFP-KRAB iPSCs expressing HP1α sgRNA into neurons, iPSCs were dissociated by using Accutase (#AT-104, Innovative Cell Technologies) and then seeded onto dishes coated with Matrigel (354230, Corning). Three days after differentiation, cells were dissociated by using Accutase and then seeded onto poly-L-ornithine–coated plates (6-well plate) or glass coverslips (24-well plate) at a density of 7×10^5 or 2×10^4 cells per well, respectively. Six days later, the neurons were fixed with 4% paraformaldehyde for immunofluorescence staining or harvested for Western blot and qPCR analyses.

Statistics

Data are presented as the mean ± the standard error of the mean (SEM) and analyzed with a two-tailed unpaired *t* test or one-way or two-way analysis of variance (ANOVA) followed by Tukey's post hoc analysis (Prism statistical software). End points of interest [i.e., body weight, brain weight, poly(PR)-positive cells, poly(PR) expression, NeuN-positive cortical neurons, Purkinje cell density, transgene RNA levels, *Gfap* and *CD68* mRNA expression, and Gfap and CD68 immunopositivity] were compared between male and female mice within each cohort. Other than body weight, no sex differences were observed. With the exception of body weight, analyses were performed on all mice within a given cohort. Data are presented such as to distinguish male and female mice; male mice are represented by solid symbols on dot plots, and female mice by empty symbols. Statistical analysis of RNA-seq data is described in the section RNA-seq, Gene Ontology, and RE analyses.

REFERENCES AND NOTES

1. M. DeJesus-Hernandez *et al*., Expanded GGGGCC hexanucleotide repeat in noncoding region of C9ORF72 causes chromosome 9p-linked FTD and ALS. *Neuron* **72**, 245–256 (2011). doi: 10.1016/j.neuron.2011.09.011; pmid: 21944778
2. A. E. Renton *et al*., A hexanucleotide repeat expansion in C9ORF72 is the cause of chromosome 9p21-linked ALS-FTD. *Neuron* **72**, 257–268 (2011). doi: 10.1016/j.neuron.2011.09.010; pmid: 21944779
3. J. G. O'Rourke *et al*., C9orf72 is required for proper macrophage and microglial function in mice. *Science* **351**, 1324–1329 (2016). doi: 10.1126/science.aaf1064; pmid: 26989253
4. A. Burberry *et al*., Loss-of-function mutations in the C9ORF72 mouse ortholog cause fatal autoimmune disease. *Sci. Transl. Med.* **8**, 347ra93 (2016). doi: 10.1126/scitranslmed.aaf6038; pmid: 27412785
5. C. Sellier *et al*., Loss of C9ORF72 impairs autophagy and synergizes with polyQ Ataxin-2 to induce motor neuron dysfunction and cell death. *EMBO J.* **35**, 1276–1297 (2016). doi: 10.15252/embj.201593350; pmid: 27103069
6. M. Yang *et al*., A C9ORF72/SMCR8-containing complex regulates ULK1 and plays a dual role in autophagy. *Sci. Adv.* **2**, e1601167 (2016). doi: 10.1126/sciadv.1601167; pmid: 27617292
7. C. P. Webster *et al*., The C9orf72 protein interacts with Rab1a and the ULK1 complex to regulate initiation of autophagy. *EMBO J.* **35**, 1656–1676 (2016). doi: 10.15252/embj.201694401; pmid: 27334615
8. P. M. Sullivan *et al*., The ALS/FTLD associated protein C9orf72 associates with SMCR8 and WDR41 to regulate the autophagy-lysosome pathway. *Acta Neuropathol. Commun.* **4**, 51 (2016). doi: 10.1186/s40478-016-0324-5; pmid: 27193190
9. Y. Shi *et al*., Haploinsufficiency leads to neurodegeneration in C9ORF72 ALS/FTD human induced motor neurons. *Nat. Med.* **24**, 313–325 (2018). doi: 10.1038/nm.4490; pmid: 29400714
10. C. J. Donnelly *et al*., RNA toxicity from the ALS/FTD C9ORF72 expansion is mitigated by antisense intervention. *Neuron* **80**, 415–428 (2013). doi: 10.1016/j.neuron.2013.10.015; pmid: 24139042
11. J. Cooper-Knock *et al*., Sequestration of multiple RNA recognition motif-containing proteins by C9orf72 repeat expansions. *Brain* **137**, 2040–2051 (2014). doi: 10.1093/brain/awu120; pmid: 24866055
12. D. Sareen *et al*., Targeting RNA foci in iPSC-derived motor neurons from ALS patients with a C9ORF72 repeat expansion. *Sci. Transl. Med.* **5**, 208ra149 (2013). doi: 10.1126/scitranslmed.3007529; pmid: 24154603
13. Y. B. Lee *et al*., Hexanucleotide repeats in ALS/FTD form length-dependent RNA foci, sequester RNA binding proteins, and are neurotoxic. *Cell Rep.* **5**, 1178–1186 (2013). doi: 10.1016/j.celrep.2013.10.049; pmid: 24290757
14. K. Mori *et al*., hnRNP A3 binds to GGGGCC repeats and is a constituent of p62-positive/TDP43-negative inclusions in the hippocampus of patients with C9orf72 mutations. *Acta Neuropathol.* **125**, 413–423 (2013). doi: 10.1007/s00401-013-1088-7; pmid: 23381195
15. K. Zhang *et al*., The C9orf72 repeat expansion disrupts nucleocytoplasmic transport. *Nature* **525**, 56–61 (2015). doi: 10.1038/nature14973; pmid: 26308891
16. B. D. Freibaum *et al*., GGGGCC repeat expansion in C9orf72 compromises nucleocytoplasmic transport. *Nature* **525**, 129–133 (2015). doi: 10.1038/nature14974; pmid: 26308899
17. A. S. Burguete *et al*., GGGGCC microsatellite RNA is neuritically localized, induces branching defects, and perturbs transport granule function. *eLife* **4**, e08881 (2015). doi: 10.7554/eLife.08881; pmid: 26650351
18. P. E. Ash *et al*., Unconventional translation of C9ORF72 GGGGCC expansion generates insoluble polypeptides specific to c9FTD/ALS. *Neuron* **77**, 639–646 (2013). doi: 10.1016/j.neuron.2013.02.004; pmid: 23415312
19. T. F. Gendron *et al*., Antisense transcripts of the expanded C9ORF72 hexanucleotide repeat form nuclear RNA foci and undergo repeat-associated non-ATG translation in c9FTD/ALS. *Acta Neuropathol.* **126**, 829–844 (2013). doi: 10.1007/s00401-013-1192-8; pmid: 24129584
20. K. Mori *et al*., Bidirectional transcripts of the expanded C9orf72 hexanucleotide repeat are translated into aggregating dipeptide repeat proteins. *Acta Neuropathol.* **126**, 881–893 (2013). doi: 10.1007/s00401-013-1189-3; pmid: 24132570
21. K. Mori *et al*., The C9orf72 GGGGCC repeat is translated into aggregating dipeptide-repeat proteins in FTLD/ALS. *Science* **339**, 1335–1338 (2013). doi: 10.1126/science.1232927; pmid: 23393093
22. T. Zu *et al*., RAN proteins and RNA foci from antisense transcripts in C9ORF72 ALS and frontotemporal dementia. *Proc. Natl. Acad. Sci. U.S.A.* **110**, E4968–E4977 (2013). doi: 10.1073/pnas.1315438110; pmid: 24248382
23. I. Kwon *et al*., Poly-dipeptides encoded by the C9orf72 repeats bind nucleoli, impede RNA biogenesis, and kill cells. *Science* **345**, 1139–1145 (2014). doi: 10.1126/science.1254917; pmid: 25081482
24. X. Wen *et al*., Antisense proline-arginine RAN dipeptides linked to C9ORF72-ALS/FTD form toxic nuclear aggregates that initiate in vitro and in vivo neuronal death. *Neuron* **84**, 1213–1225 (2014). doi: 10.1016/j.neuron.2014.12.010; pmid: 25521377
25. S. Mizielinska *et al*., C9orf72 repeat expansions cause neurodegeneration in *Drosophila* through arginine-rich proteins. *Science* **345**, 1192–1194 (2014). doi: 10.1126/science.1256800; pmid: 25103406
26. K. H. Lee *et al*., C9orf72 dipeptide repeats impair the assembly, dynamics, and function of membrane-less organelles. *Cell* **167**, 774–788.e17 (2016). doi: 10.1016/j.cell.2016.10.002; pmid: 27768896
27. K. Y. Shi *et al*., Toxic PR_n poly-dipeptides encoded by the *C9orf72* repeat expansion block nuclear import and export. *Proc. Natl. Acad. Sci. U.S.A.* **114**, E1111–E1117 (2017). doi: 10.1073/pnas.1620293114; pmid: 28069952
28. A. Jovičić *et al*., Modifiers of C9orf72 dipeptide repeat toxicity connect nucleocytoplasmic transport defects to FTD/ALS. *Nat. Neurosci.* **18**, 1226–1229 (2015). doi: 10.1038/nn.4085; pmid: 26308983
29. N. J. Kramer *et al*., CRISPR-Cas9 screens in human cells and primary neurons identify modifiers of C9ORF72 dipeptide-repeat-protein toxicity. *Nat. Genet.* **50**, 603–612 (2018). doi: 10.1038/s41588-018-0070-7; pmid: 29507424
30. Z. Tao *et al*., Nucleolar stress and impaired stress granule formation contribute to C9orf72 RAN translation-induced cytotoxicity. *Hum. Mol. Genet.* **24**, 2426–2441 (2015). doi: 10.1093/hmg/ddv005; pmid: 25575510
31. K. Kanekura *et al*., Poly-dipeptides encoded by the C9ORF72 repeats block global protein translation. *Hum. Mol. Genet.* **25**, 1803–1813 (2016). doi: 10.1093/hmg/ddw052; pmid: 26931465
32. S. Boeynaems *et al*., Phase separation of C9orf72 dipeptide repeats perturbs stress granule dynamics. *Mol. Cell* **65**, 1044–1055.e5 (2017). doi: 10.1016/j.molcel.2017.02.013; pmid: 28306503
33. I. R. Mackenzie *et al*., Quantitative analysis and clinico-pathological correlations of different dipeptide repeat protein pathologies in C9ORF72 mutation carriers. *Acta Neuropathol.* **130**, 845–861 (2015). doi: 10.1007/s00401-015-1476-2; pmid: 26374446
34. S. C. Vatsavayai *et al*., Timing and significance of pathological features in C9orf72 expansion-associated frontotemporal dementia. *Brain* **139**, 3202–3216 (2016). doi: 10.1093/brain/aww250; pmid: 27797809
35. J. C. Eissenberg, S. C. Elgin, HP1a: a structural chromosomal protein regulating transcription. *Trends Genet.* **30**, 103–110 (2014). doi: 10.1016/j.tig.2014.01.002; pmid: 24555990
36. B. van Steensel, A. S. Belmont, Lamina-associated domains: Links with chromosome architecture, heterochromatin, and gene repression. *Cell* **169**, 780–791 (2017). doi: 10.1016/j.cell.2017.04.022; pmid: 28525751
37. S. H. Kwon, J. L. Workman, The changing faces of HP1: From heterochromatin formation and gene silencing to euchromatic gene expression. *Bioessays* **33**, 280–289 (2011). doi: 10.1002/bies.201000138; pmid: 21271610
38. T. Dechat *et al*., Nuclear lamins: Major factors in the structural organization and function of the nucleus and chromatin. *Genes Dev.* **22**, 832–853 (2008). doi: 10.1101/gad.1652708; pmid: 18381888
39. Y. J. Zhang *et al*., Poly(GR) impairs protein translation and stress granule dynamics in C9orf72-associated frontotemporal dementia and amyotrophic lateral sclerosis. *Nat. Med.* **24**, 1136–1142 (2018). doi: 10.1038/s41591-018-0071-1; pmid: 29942091
40. B. Frost, F. H. Bardai, M. B. Feany, Lamin dysfunction mediates neurodegeneration in tauopathies. *Curr. Biol.* **26**, 129–136 (2016). doi: 10.1016/j.cub.2015.11.039; pmid: 26725200
41. D. K. Shumaker *et al*., Mutant nuclear lamin A leads to progressive alterations of epigenetic control in premature aging. *Proc. Natl. Acad. Sci. U.S.A.* **103**, 8703–8708 (2006). doi: 10.1073/pnas.0602569103; pmid: 16738054
42. P. Scaffidi, T. Misteli, Reversal of the cellular phenotype in the premature aging disease Hutchinson-Gilford progeria syndrome. *Nat. Med.* **11**, 440–445 (2005). doi: 10.1038/nm1204; pmid: 15750600
43. A. G. Larson *et al*., Liquid droplet formation by HP1α suggests a role for phase separation in heterochromatin. *Nature* **547**, 236–240 (2017). doi: 10.1038/nature22822; pmid: 28636604

44. A. R. Strom *et al*., Phase separation drives heterochromatin domain formation. *Nature* **547**, 241–245 (2017). doi: 10.1038/nature22989; pmid: 28636597
45. M. Prudencio *et al*., Distinct brain transcriptome profiles in C9orf72-associated and sporadic ALS. *Nat. Neurosci.* **18**, 1175–1182 (2015). doi: 10.1038/nn.4065; pmid: 26192745
46. D. A. Mordes *et al*., Dipeptide repeat proteins activate a heat shock response found in C9ORF72-ALS/FTLD patients. *Acta Neuropathol. Commun.* **6**, 55 (2018). doi: 10.1186/s40478-018-0555-8; pmid: 29973287
47. N. Saksouk, E. Simboeck, J. Déjardin, Constitutive heterochromatin formation and transcription in mammals. *Epigenetics Chromatin* **8**, 3 (2015). doi: 10.1186/1756-8935-8-3; pmid: 25788984
48. M. Prudencio *et al*., Repetitive element transcripts are elevated in the brain of C9orf72 ALS/FTLD patients. *Hum. Mol. Genet.* **26**, 3421–3431 (2017). doi: 10.1093/hmg/ddx233; pmid: 28637276
49. L. Krug *et al*., Retrotransposon activation contributes to neurodegeneration in a *Drosophila* TDP-43 model of ALS. *PLOS Genet.* **13**, e1006635 (2017). doi: 10.1371/journal.pgen.1006635; pmid: 28301478
50. T. K. Saldi *et al*., TDP-1, the *Caenorhabditis elegans* ortholog of TDP-43, limits the accumulation of double-stranded RNA. *EMBO J.* **33**, 2947–2966 (2014). doi: 10.15252/embj.201488740; pmid: 25391662
51. T. Sijen, R. H. Plasterk, Transposon silencing in the *Caenorhabditis elegans* germ line by natural RNAi. *Nature* **426**, 310–314 (2003). doi: 10.1038/nature02107; pmid: 14628056
52. T. K. Saldi *et al*., The *Caenorhabditis elegans* ortholog of TDP-43 regulates the chromatin localization of the heterochromatin protein 1 homolog HPL-2. *Mol. Cell. Biol.* **38**, e00668-17 (2018). doi: 10.1128/MCB.00668-17; pmid: 29760282
53. L. A. Gilbert *et al*., CRISPR-mediated modular RNA-guided regulation of transcription in eukaryotes. *Cell* **154**, 442–451 (2013). doi: 10.1016/j.cell.2013.06.044; pmid: 23849981
54. L. A. Gilbert *et al*., Genome-scale CRISPR-mediated control of gene repression and activation. *Cell* **159**, 647–661 (2014). doi: 10.1016/j.cell.2014.09.029; pmid: 25307932
55. R. Tian, M. A. Gachechiladze, C. H. Ludwig, M. T. Laurie, J. Y. Hong, D. Nathaniel, A. V. Prabhu, M. S. Fernandopulle, R. Patel, M. E. Ward, M. Kampmann, CRISPR-based platform for multimodal genetic screens in human iPSC-derived neurons. bioRxiv 513309 [Preprint]. 7 January 2019. doi: 10.1101/513309
56. Y. J. Zhang *et al*., C9ORF72 poly(GA) aggregates sequester and impair HR23 and nucleocytoplasmic transport proteins. *Nat. Neurosci.* **19**, 668–677 (2016). doi: 10.1038/nn.4272 pmid: 26998601
57. S. Rodriguez, B. R. Schrank, A. Sahin, H. Al-Lawati, I. Constantino, E. Benz, D. Fard, A. D. Albers, L. Cao, A. C. Gomez, E. Ratti, M. Cudkowicz, M. P. Frosch, M. Talkowski, P. K. Sorger, B. T. Hyman, M. W. Albers, Genome-encoded cytoplasmic double-stranded RNAs, found in C9ORF72 ALS-FTD brain, provoke propagated neuronal death. bioRxiv 248328 [Preprint]. 19 January 2018. . doi: 10.1101/248328
58. H. Tan *et al*., Retrotransposon activation contributes to fragile X premutation rCGG-mediated neurodegeneration. *Hum. Mol. Genet.* **21**, 57–65 (2012). doi: 10.1093/hmg/ddr437; pmid: 21940752
59. Y. J. Zhang *et al*., Aggregation-prone c9FTD/ALS poly(GA) RAN-translated proteins cause neurotoxicity by inducing ER stress. *Acta Neuropathol.* **128**, 505–524 (2014). doi: 10.1007/s00401-014-1336-5; pmid: 25173361
60. M. A. Horlbeck *et al*., Compact and highly active next-generation libraries for CRISPR-mediated gene repression and activation. *eLife* **5**, e19760 (2016). doi: 10.7554/eLife.19760; pmid: 27661255
61. National Research Council Committee for the Update of the Guide for the Care and Use of Laboratory Animals, *Guide for the Care and Use of Laboratory Animals* (National Academies, ed. 8, 2011).
62. C. Wang *et al*., Scalable production of iPSC-derived human neurons to identify Tau-lowering compounds by high-content screening. *Stem Cell Reports* **9**, 1221–1233 (2017). doi: 10.1016/j.stemcr.2017.08.019; pmid: 28966121
63. M. S. Fernandopulle *et al*., Transcription factor-mediated differentiation of human iPSCs into neurons. *Curr. Protoc. Cell Biol.* **79**, e51 (2018). doi: 10.1002/cpcb.51; pmid: 29924488

ACKNOWLEDGMENTS

We are grateful to all patients who agreed to donate postmortem tissue. **Funding:** This work was supported by the National Institutes of Health National Institute of Neurological Disorders and Stroke [grants R35NS097273 (L.P.), P01NS084974 (L.P., D.W. D., R.R., and B.O.), P01NS099114 (T.F.G. and L.P.), R01NS088689 (L.P.), R01NS063964 (C.D.L.), and U54NS100717 (M.K.)]; the National Institutes of Health National Institute on Aging [grants R01AG062359 and R56AG057528 (M.K.)]; the National Institutes of Health National Institute of General Medical Sciences [grant DP2GM119139 (M.K.)]; the Mayo Clinic Foundation (L.P.); the Amyotrophic Lateral Sclerosis Association (T.F.G., L.P., Y.-J.Z., and M.P.); the Robert Packard Center for ALS Research at Johns Hopkins (L.P. and J.S.); and the Target ALS Foundation (T.F.G., L.G., L.P., J.S., and Y.-J.Z.). **Author contributions:** Y.-J.Z. and L.P. contributed to the conception and design. Y.-J.Z. made plasmids; prepared lysates; performed Western blotting, qPCR, and immunofluorescence staining; purified recombinant proteins; and cultured iPSCs. L.G. and J.S. contributed to in vitro DPR peptide and HP1α assays. C.L., R.T., M.A.G., M.E.W., and M.K. developed CRISPRi technology in iPSC-derived neurons and provided unpublished reagents. P.K.G. and C.D.L analyzed RNA-seq data. T.F.G. and L.M.D. generated and/or performed poly(PR) immunoassays. A.D.O. performed intracerebroventricular injections, behavioral tests, immunofluorescence staining, and quantification of neuropathology. K.J.-W. performed electrophoretic mobility shift assays and made plasmids and AAV1 virus. Y.W. performed quantification of neuropathology. S.R.P. and Y.W. contributed to the generation of iPSCs. M.P. and Y.S. performed qPCR and used the RNA 6000 Nano kit to verify RNA integrity. J.C. performed intracerebroventricular injections. M.D. and W.-L.L. performed electron microscopy and immunoelectron microscopy, respectively. J.T. collected mouse tissues. M.Y. prepared lysates. M.C.-C. performed immunohistochemistry. Y.C. and J.W.A. purified recombinant proteins. A.K. and J.D.F contributed to behavioral tests. A.D., G.A., and A.M. made mouse monoclonal anti-PR antibody. R.R., B.O., and D.W.D. contributed to the collection and genotyping of human tissues. Y.-J.Z., T.F.G., L.G., J.S., and L.P. analyzed data and wrote the manuscript. **Competing interests:** B.O. served as a paid consultant for Flex Pharma, Mitsubishi Tanabe, and Biogen Idec. G.A. and A.M. are full-time employees of and own equity in Biogen Idec. M.K. serves on the scientific advisory board of Engine Biosciences and is a consultant for Maze Therapeutics. M.K. has filed a patent application related to CRISPRi and CRISPRa screening (PCT/US15/40449). Other authors declare no competing financial interests. **Data and material availability:** All data are available in the main text or the supplementary materials. The materials that support the findings of this study are available from the corresponding author upon reasonable request. The Gene Expression Omnibus accession number of RNA-seq data is GSE124834.

SUPPLEMENTARY MATERIALS

www.sciencemag.org/content/363/6428/eaav2606/suppl/DC1
Materials and Methods
Figs. S1 to S8
Tables S1 to S7
References (*64*–*67*)
Movies S1 and S2
Datasets S1 and S2

2 September 2018; resubmitted 7 December 2018
Accepted 14 January 2019
10.1126/science.aav2606

Science

Heterochromatin anomalies and double-stranded RNA accumulation underlie *C9orf72* poly(PR) toxicity

Yong-Jie Zhang, Lin Guo, Patrick K. Gonzales, Tania F. Gendron, Yanwei Wu, Karen Jansen-West, Aliesha D. O'Raw, Sarah R. Pickles, Mercedes Prudencio, Yari Carlomagno, Mariam A. Gachechiladze, Connor Ludwig, Ruilin Tian, Jeannie Chew, Michael DeTure, Wen-Lang Lin, Jimei Tong, Lillian M. Daughrity, Mei Yue, Yuping Song, Jonathan W. Andersen, Monica Castanedes-Casey, Aishe Kurti, Abhishek Datta, Giovanna Antognetti, Alexander McCampbell, Rosa Rademakers, Björn Oskarsson, Dennis W. Dickson, Martin Kampmann, Michael E. Ward, John D. Fryer, Christopher D. Link, James Shorter and Leonard Petrucelli

Science **363** (6428), eaav2606.
DOI: 10.1126/science.aav2606

How dipeptide repeats cause pathology

A repeat expansion in the chromosome 9 open reading frame 72 (*C9orf72*) gene is the most common known cause of two neurodegenerative diseases: frontotemporal dementia and amyotrophic lateral sclerosis. This expansion leads to the abnormal production of proteins of repeating dipeptides, but their contribution to disease pathogenesis remains unclear. Zhang *et al.* engineered a mouse model to study the consequences of one of these dipeptides—prolinearginine dipeptide repeat protein, poly(PR)—in the brain. They found that poly(PR) caused neuron loss as well as motor and memory impairments. These detrimental effects resulted from poly(PR)-induced perturbation of heterochromatin function, a tightly packed form of DNA that represses gene expression.

Science, this issue p. eaav2606